Rock Mechanics and Rock Engineering (2020) 53:3237–3252
https://doi.org/10.1007/s00603-020-02099-y

ORIGINAL PAPER

Lower Bound Limit Analysis Using Power Cone Programming for Solving Stability Problems in Rock Mechanics for Generalized Hoek–Brown Criterion

Jyant Kumar[1] · **Obaidur Rahaman**[1]

Received: 1 July 2019 / Accepted: 24 March 2020 / Published online: 11 April 2020

Abstract
This study introduces a methodology to solve plane strain stability problems in rock mechanics, following the generalized Hoek and Brown yield criterion, by employing the lower bound finite elements limit analysis in conjunction with the power cone programming. The efficacy of the proposed approach has been demonstrated by solving three different types of stability problems: (1) finding the bearing capacity of strip footings on rock media, (2) assessing the stability of finite rock slopes, and (3) the stability analysis of unlined rectangular tunnels in rock mass. In all the cases, the results obtained from the analysis have been compared thoroughly with that computed using (1) nonlinear programming, and (2) semi-definite programming technique. The present approach has been found to be computationally very robust and it generates very accurate solutions.

Keywords Limit analysis · Rock mechanics · Finite elements · Power cone programming · Hoek and Brown yield criterion

List of Symbols

σ_1	Major principal stress
σ_3	Minor principal stress
σ_{ci}	Uniaxial compressive strength
m_{b}	Hoek–Brown material constant
m_i	Hoek–Brown material constant
s	Hoek–Brown material constant
α	Hoek–Brown material constant
GSI	Geological strength index
D	Disturbance factor
$\mathcal{K}$	Cone
$\mathcal{K}^*$	Dual cone
$\mathfrak{R}^n$	n-Dimensional real space
$\mathfrak{R}^{m\times n}$	Real matrices of size $m \times n$
Q^n	n-Dimensional quadratic cone
Q_r^n	n-Dimensional rotated quadratic cone
P_n^β	n-Dimensional power cone
$\mathbf{S}^n$	Set of $n \times n$ symmetric matrices
$\mathbf{S}_+^n$	Set of $n \times n$ positive definite matrices
$\boldsymbol{\sigma}$	Stress tensor
$\lambda_{\max}$	Auxiliary variable
$\lambda_{\min}$	Auxiliary variable
t	Auxiliary variable
σ_x	Normal stress on x-plane
σ_y	Normal stress on y-plane
τ_{xy}	Shear stress on x-plane in y-direction
$\boldsymbol{c}$	Vector which contains the objective function
$\bar{\boldsymbol{\sigma}}$	Global unknown vector
NN	Number of nodes
$\mathbf{A}_{\mathrm{equi}}$	Matrix containing the left-hand side of all the equilibrium equations
$\mathbf{A}_{\mathrm{dis}}$	Matrix containing the left-hand side of all the discontinuity equations
$\mathbf{A}_{\mathrm{bc}}$	Matrix containing the left-hand side of all the boundary conditions
$\mathbf{b}_{\mathrm{equi}}$	Vector containing the right-hand side of all the equilibrium equations
$\mathbf{b}_{\mathrm{dis}}$	Vector containing the right-hand side of all the discontinuity equations
$\mathbf{b}_{\mathrm{bc}}$	Vector containing the right-hand side of all the boundary conditions
B	Width of foundation
Q_{u}	Maximum vertical load
N_σ	Bearing capacity factor of strip footing in weightless media
$N_{\sigma\gamma}$	Bearing capacity factor of strip footing
q_{u}	Ultimate bearing pressure
γ	Unit weight of rock mass

✉ Jyant Kumar
jkumar@iisc.ac.in

[1] Department of Civil Engineering, Indian Institute of Science, Bengaluru 560012, India

L	Parameter which defines the boundary
H	Parameter which defines the boundary
p	Parameter which defines the state of stress
q	Parameter which defines the state of stress
β	Slope angle
N_s	Stability number for slope
h	Height of tunnel
w	Width of tunnel
N_t	Stability number for tunnel

1 Introduction

To solve different stability analysis in rock mechanics, two different computational approaches, namely, (1) the continuum-based formulations (Zienkiewicz et al. 1975; Swan and Seo 1999; Li et al. 2009), and (2) discontinuum-based formulations (Cundall 1971; Shi and Goodman 1985), are often employed. The elasto-plastic finite element method (FEM) is often adopted while employing the continuum-based approaches. In this approach, for determining the stability of any structure, the associated analysis is based on either (1) the shear strength reduction method (SSRM) (Zienkiewicz et al. 1975), or (2) the gravity increase method (GIM) (Swan and Seo 1999; Li et al. 2009; Lian et al. 2018). In the SSRM, for given imposed loading on the structure, the material shear strength parameters are gradually reduced/increased to induce the onset of ultimate shear failure. Similarly, in the GIM, the value of gravitational acceleration is increased/reduced to attain the onset of ultimate shear failure; this analysis is very similar to the experimental approach used typically in a centrifuge test (Alzoubi et al. 2010). The factor of safety, accordingly, is defined as the ratio of the (1) required shear strength parameters to induce the failure to the given material shear strength parameters in the SSRM, (2) required gravitational acceleration to generate the failure to the acceleration (g) due to gravity in GIM. For jointed rock masses, the analysis is often dictated by the shear strength along the rock joints and the discontinuum-based techniques, for instance, the discrete element method (DEM) (Cundall 1971) and the discontinuous deformation analysis (DDA) (Shi and Goodman 1985) can be employed to solve the problem. The SSRM- and GIM-based analyses can be even used for the discontinuum-based methods as well. With the advancement of the finite element method and different robust optimization techniques, the *finite element limit analysis* (FELA) has emerged as a very powerful tool for solving various stability problems in soils and rocks (Sloan 1988; Merifield et al. 2006; Krabbenhoft et al. 2007). The FELA does not require any assumption associated with the geometry of the collapse mechanism. It can deal with complicated boundary conditions, arbitrary geometries, anisotropy and heterogeneity of the material; the domain is always discretized into a large number of elements and the heterogeneity as well as anisotropy of the material can be easily accounted in the analysis by defining the relevant input material parameters to the different elements in the domain. Unlike the elasto-plastic FEM, in the FELA, there is no need to describe the complete constitutive model since the method uses only the shear strength parameters at failure. The solution obtained using the FELA is bracketed into two bounds, namely, lower and upper bounds. It should be mentioned that the computational cost in the FELA remains much smaller than the elasto-plastic FEM as the later technique tends to generate the complete load–deformation plot before attaining the failure (Makrodimopoulos and Martin 2006; Sloan 2013).

For problems involving rock mass, the *generalized Hoek and Brown* (GHB) yield criterion is often applied to check failure in intact and jointed rock mass. This failure criterion was originally developed by Hoek and Brown (1980) and Hoek (1983), through curve-fitting of laboratory triaxial test data on rock samples, and it was later modified by Hoek et al. (2002). In the FELA, the GHB has also been employed to solve different stability problems in rock media. At present, the associated optimization problems using the GHB have been solved mostly with the usage of the *nonlinear programming* (NLP). For instance (1) the determination of bearing capacity of strip and circular footings on rock media (Merifield et al. 2006; Chakraborty and Kumar 2015), (2) the stability of rock slopes (Li et al. 2008) and (3) the stability of underground openings in rock mass (Suchowerska et al. 2012; Zhang et al. 2019). To use the NLP, the yield function needs to be C^2 continuous, that is, the second derivative of the yield function needs to be continuous. However, in principal stress space, the GHB yield criterion has a form of pyramid with the sharp edges. The stress discontinuities appear at the apex of the yield surface in a meridian-plane, and along the corners of the hexagon in a pi-plane. To implement the NLP algorithm for the HB yield criterion, these discontinuities need to be smoothed. The different conic programming techniques such as *semi-definite programming* (SDP), *second-order cone programming* (SOCP) and *power cone programming* (PCP) can easily handle any yield function, even with the singularities, provided the yield surface remains convex and can be expressed in the form of conic constraints. As compared to the NLP, the different conic programming techniques which often employ the primal–dual interior-point algorithms (Nesterov and Todd 1998; Andersen et al. 2003), have been proven to be far superior, both in terms of accuracy and computational efficiency (Krabbenhoft et al. 2007; Makrodimopoulos and Martin 2006). In a recent study, while using the LB-FELA, Kumar and Mohapatra (2017) have employed the SDP technique while solving the plane strain and axisymmetric problems using the modified Hoek–Brown (MHB) yield criterion

in which case the value of the exponent (α) needs to be kept equal to 0.5. This assumption leads to much higher values of the collapse load(s), especially when the magnitude of the geological strength index (GSI) becomes lesser than 30. A trial and iterative procedure was later introduced by Kumar and Mohapatra (2018) to extend this work on the basis of the SDP to account for any given value of α. Using the same SDP formulation, again with $\alpha = 0.5$, Ukritchon and Keawsawasvong (2018) provided the solution for the three-dimensional problem. Ukritchon and Keawsawasvong (2019) have determined the stability numbers of an unlined square tunnel on the basis of the plane strain analysis. However, due to an assumption of $\alpha = 0.5$, the usage of the SDP in the LB-FELA fails to capture the exact non-linear nature of the GHB.

In the present research, a plane strain LB-FELA formulation has been presented while implementing the exact form of the GHB criterion in rock mass with the usage of the power cone programming (PCP): a relatively new technique in the field of optimization. The need of any kind of the modification of the GHB yield surface has been totally eliminated. For the purpose of checking the efficacy and accuracy of the proposed formulation, three different types of stability problems in rock mechanics have been solved: (1) finding the bearing capacity of strip footings on horizontal rock media, (2) assessing the stability of finite rock slopes, and (3) determining the stability of rectangular unlined tunnels in rock mass. For all the selected problems, the results obtained from the present analysis have been thoroughly compared with that reported in literature.

2 Hoek and Brown (HB) Yield Criterion

The Hoek–Brown failure criterion was initially proposed by Hoek and Brown (1980). After a number of subsequent modifications, the generalized Hoek–Brown (GHB) yield criterion (Hoek et al. 2002; Hoek 2007) is recommended for defining the failure in rock mass. If tensile normal stresses are considered as positive, this criterion has the following mathematical form:

$$\sigma_1 - \sigma_3 - \left(-m_b\sigma_1\left(-\sigma_{ci}\right)^{(1-\alpha)/\alpha} + s\left(-\sigma_{ci}\right)^{1/\alpha}\right)^{\alpha} \leq 0, \quad (1)$$

where σ_1 and σ_3 refer to the major (maximum tensile/minimum compressive) and minor (minimum tensile/maximum compressive) principal stresses, and σ_{ci} defines the uniaxial compressive strength of rock samples. The other material parameters, namely, m_b, s and α become a function of geological strength index (GSI), disturbance factor (D) and the parameter (m_i), as defined by the following expressions:

$$m_b = m_i \exp\left(\frac{\mathrm{GSI} - 100}{28 - 14D}\right), \quad (2a)$$

$$s = \exp\left(\frac{\mathrm{GSI} - 100}{9 - 3D}\right), \quad (2b)$$

$$\alpha = \frac{1}{2} + \frac{1}{6}(\exp(-\mathrm{GSI}/15) - \exp(-20/3)). \quad (2c)$$

3 Conic Optimization Techniques

The applications of *second-order cone programming* (SOCP) and *semi-definite programming* (SDP) techniques in the FELA allow nonlinear inequality constraints to be expressed in the form of (1) either a set of quadratic cones or rotated quadratic cones in SOCP (Mohapatra and Kumar 2019a), and (2) the cones of positive semidefinite matrices in the SDP (Alizadeh 1995; Alizadeh and Goldfarb 2003; Mohapatra and Kumar 2019b). These conic programming techniques eliminate completely the requirement of either the linearization or smoothing of the nonlinear yield surface which is otherwise needed in the *nonlinear programming* (NLP) method.

A set $\mathcal{K}$ is defined as a cone if for any $\mathbf{x} \in \mathcal{K}$ and with $\mu \geq 0$, $\mu\boldsymbol{x} \in \mathcal{K}$. The set $\mathcal{K}$ is a convex cone if it remains convex for every $\mathbf{x}$ and $\mathbf{y} \in \mathcal{K}$ and with μ and $\in \geq 0$, $\mu\mathbf{x} + \in \mathbf{y} \in \mathcal{K}$. The quadratic cone, power cone and semidefinite cones are the standard examples of convex cones. A quadratic cone is defined as:

$$\mathcal{K} \equiv Q^n = \left\{\mathbf{x} \in \Re^n | \sqrt{x_2^2 + x_3^2 + \ldots \ldots x_n^2} \leq x_1, x_1 \geq 0\right\}. \quad (3)$$

The convex cone in the following form is known as a rotated quadratic cone:

$$\mathcal{K} \equiv Q_r^n = \left\{\mathbf{x} \in \Re^n | x_3^2 + x_4^2 + \ldots \ldots x_n^2 \leq 2x_1x_2; x_1, x_2 \geq 0\right\}. \quad (4)$$

The power cone is defined as:

$$\mathcal{K} \equiv P_n^{\beta} = \left\{\mathbf{x} \in \Re^n | \sqrt{x_3^2 + x_4^2 + \ldots \ldots x_n^2} \leq x_1^{\beta} x_2^{1-\beta}; 0 < \beta < 1 \text{ and} x_1, x_2 \geq 0\right\}. \quad (5)$$

Note that for the values of β equal to 0 and 1, the power cone simply takes the form of the second-order cone.

A set of $n \times n$ symmetric matrices ($\mathbf{S}^n$) are positive semidefinite if

$$\mathbf{S}_+^n = \{\mathbf{X} \in \mathbf{S}^n | \mathbf{X} \succcurlyeq 0\}. \quad (6)$$

The primal form of a standard conic programming problem can be written as:

$$(\mathrm{P}) \quad \left\{\min \mathbf{c}^{\mathrm{T}}\mathbf{x} | \mathbf{A}\mathbf{x} = \mathbf{b}, \mathbf{x} \in \mathcal{K}\right\}, \tag{7a}$$

where $\mathbf{x}^{\mathrm{T}} \in \Re^n, \mathbf{c} \in \Re^n, \mathbf{b} \in \Re^m, \mathbf{A} \in \Re^{m \times n}$ and $\mathcal{K}$ = convex cone. The dual of this conic problem is:

$$(\mathrm{D}) \quad \left\{\max \mathbf{b}^{\mathrm{T}}\mathbf{y} | \mathbf{A}^{\mathrm{T}}\mathbf{y} + \mathbf{s} = \mathbf{c}, \mathbf{s} \in \mathcal{K}^*\right\}, \tag{7b}$$

where $\mathcal{K}^* = \left\{\mathbf{s} \in \Re^n | \mathbf{s}^{\mathrm{T}}\mathbf{x} \geq 0, \forall \mathbf{x} \in \mathcal{K}\right\}$ is the dual cone to $\mathcal{K}$.

This conic programming problem can be sub-classified as (1) *second-order cone programming* (SOCP) if $\mathcal{K} \equiv Q^n$ (the quadratic cone) or Q_r^n (the rotated quadratic cone), (2) *power cone programming* (PCP) if $\mathcal{K} \equiv P_n^{\beta}$(power cone) and (2) *semi-definite programming* (SDP) if $\mathcal{K}$ is a positive semidefinite cone of $n \times n$ symmetric matrices (Alizadeh 1995; Alizadeh and Goldfarb 2003; Boyd and Vandenberghe 2004).

Similar to the linear programming (LP) technique, the conic programming (CP) techniques also follow the duality theorem and these problems can be solved very efficiently with the help of the primal–dual algorithms based on the interior-point method (IPM) (Andersen et al. 2003; Tang et al. 2014). Numerous solvers such as SeDuMi (Sturm 1999), SDPT3 (Tütüncü et al. 2003) and MOSEK (Mosek 2019) can be utilized to solve these CP problems in an efficient way. In the present investigation, for carrying out the optimization, the optimization toolbox MOSEK has been used because of its robustness and computational efficiency (Mosek 2019). The entire code for performing the finite elements limit analysis was written in MATLAB and no commercial software has been employed.

4 Modified Hoek–Brown Criterion in Terms of Semi-definite Conic Constraints

In the generalized Hoek–Brown criterion, the exponent α depends on GSI as per Eq. (2c). It has the maximum and minimum values of 0.59 and 0.50 corresponding to GSI equal to 10 and 100, respectively. Kumar and Mohapatra (2017) have considered a constant value of $\alpha = 0.5$ and the GHB has been renamed as the modified Hoek and Brown (MHB) yield criterion. In mathematical form, the MHB can be expressed as:

$$\sigma_1 - \sigma_3 - \left(-m_{\mathrm{b}}\sigma_1\left(-\sigma_{\mathrm{ci}}\right) + s\left(-\sigma_{\mathrm{ci}}\right)^2\right)^{0.5} \leq 0. \tag{8}$$

Assuming $a = -m_{\mathrm{b}}\left(-\sigma_{\mathrm{ci}}\right)$ and $b = s\left(-\sigma_{\mathrm{ci}}\right)^2$, the MHB criterion becomes as:

$$(\sigma_1 - \sigma_3) \leq (a\sigma_1 + b)^{0.5}. \tag{9}$$

To solve the optimization problem in LB-FELA, Kumar and Mohapatra (2017) implemented the MHB yield criterion in terms of the following two semi-definite and one rotated quadratic conic constraint constraints:

$$\lambda_{\max}\mathbf{I} - \boldsymbol{\sigma} \succcurlyeq 0; \quad \lambda_{\min}\mathbf{I} - \boldsymbol{\sigma} \preccurlyeq 0, \tag{10}$$

$$\lambda_{\mathrm{dif}}^2 \leq 2kl. \tag{11}$$

Here, $\boldsymbol{\sigma}$ is the stress tensor with σ_1 and σ_3 as maximum and minimum eigenvalues, respectively. $\lambda_{\max}$ and $\lambda_{\min}$ are two auxiliary variables such that $\lambda_{\max} \geq \sigma_1$ and $\lambda_{\min} \leq \sigma_3$. In Eq. (11) $\lambda_{\mathrm{dif}} = \lambda_{\max} - \lambda_{\min}$, $k = \left(a\lambda_{\max} + b\right)$ and $l = 0.5$; also λ_{dif} and k are non-negative.

As mentioned earlier, the exponent parameter α depends on GSI and it controls the curvature of the GHB, and fixing its value simply equal to 0.5 will never ensure the true solution. The comparison of the normalized yield surfaces, between MHB and GHB yield criteria for different GSI (10, 20, 30 and 40) and m_i (1, 10, 20 and 35) as illustrated in Fig. 1a–d, reveals that the MHB always predicts higher yield strength than the GHB, especially for the value of GSI smaller than 30. It can also be observed that with an increase in the value of GSI, the gap between the GHB and MHB yield surfaces reduces continuously and for GSI $\geq$ 40, the two surfaces almost coincide with each other. On account of this, Kumar and Mohapatra (2017) reported quite significant differences in the bearing capacity factors for strip and circular footings on the basis of the LB analysis using the SDP, especially for GSI $\leq$ 30. In an attempt to consider the true value of α, Kumar and Mohapatra (2018) proposed an iterative procedure. Although the iterative procedure improves the results, the computational time increases quite extensively with an increase in the number of iterations. Therefore, to improve the accuracy of the LB solution and the efficiency in terms of the required computational time, there is a need of a new methodology in which the GHB yield criterion must be implemented as conic constraints in its native form.

5 Generalized Hoek–Brown Criterion in Terms of Power Conic Constraints

The generalized Hoek–Brown criterion as in Eq. (1) can be expressed as:

$$(\sigma_1 - \sigma_3) \leq (a'\sigma_1 + b')^{\alpha}, \tag{12}$$

where $a' = -m_{\mathrm{b}}\sigma_1\left(-\sigma_{\mathrm{ci}}\right)^{(1-\alpha)/\alpha}$ and $b' = s\left(-\sigma_{\mathrm{ci}}\right)^{1/\alpha}$.

Now, introducing a new variable such that

$$t = (a'\sigma_1 + b')^{\alpha}. \tag{13}$$

Since $\sigma_1 > \sigma_3$, $t \geq 0$.

Hence, Eq. (12) can be re-written as:

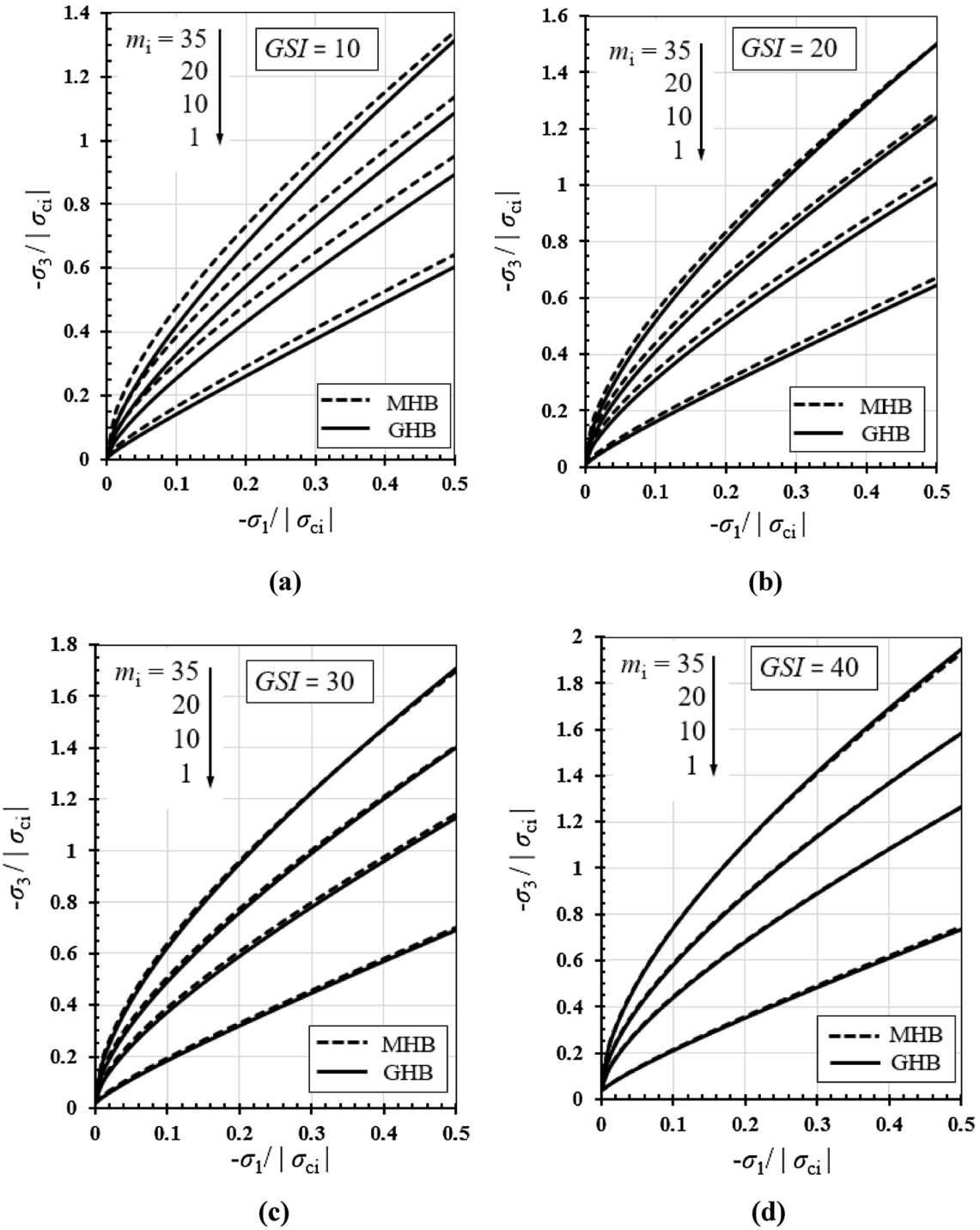

Fig. 1 A comparison of the MHB and the GHB for $D=0$ using different values of m_i with: **a** GSI= 10, **b** GSI= 20, **c** GSI= 30, **d** GSI= 40

$$\left(\sigma_1 - \sigma_3\right) \le t. \tag{14}$$

For a plane strain problem

$$\sigma_1 = \frac{\sigma_x + \sigma_y}{2} + \sqrt{\left(\frac{\sigma_x - \sigma_y}{2}\right)^2 + \left(\tau_{xy}\right)^2}, \tag{15a}$$

$$\sigma_3 = \frac{\sigma_x + \sigma_y}{2} - \sqrt{\left(\frac{\sigma_x - \sigma_y}{2}\right)^2 + \left(\tau_{xy}\right)^2}, \tag{15b}$$

$$\left(\sigma_1 - \sigma_3\right) = \sqrt{\left(\sigma_x - \sigma_y\right)^2 + \left(2\tau_{xy}\right)^2}, \tag{15c}$$

where σ_x, σ_y and τ_{xy} refer to normal and shear stresses with respect to the cartesian co-ordinates system. Therefore, Eq. (14) can be written as:

$$\sqrt{\left(\sigma_x - \sigma_y\right)^2 + \left(2\tau_{xy}\right)^2} \le t. \tag{16}$$

Since $t \ge 0$, Eq. (16) can easily be expressed in the standard form of a second-order conic constraint:

$$\sqrt{x_2^2 + x_3^2} \le x_1, \tag{17}$$

where $x_1 = t$, $x_2 = (\sigma_x - \sigma_y)$ and $x_3 = 2\tau_{xy}$.

For a plane strain case again, using Eq. (15a), the value of t in Eq. (13) can be written in terms of σ_x, σ_y and τ_{xy}:

$$t = \left[\frac{a'}{2}\left\{\left(\sigma_x + \sigma_y\right) + \sqrt{\left(\sigma_x - \sigma_y\right)^2 + \left(2\tau_{xy}\right)^2}\right\} + b'\right]^{\alpha}. \tag{18}$$

Now from Eqs. (16) and (18), since the value of the exponent α is always +ve,

$$t \le \left[\frac{a'}{2}\left\{\left(\sigma_x + \sigma_y\right) + t\right\} + b'\right]^{\alpha}. \tag{19}$$

If x_4, x_5 and x_6 are defined by the following expressions:

$$x_4 = \frac{a'}{2}\left\{\left(\sigma_x + \sigma_y\right) + t\right\} + b', \quad x_5 = 1, \quad \text{and} \quad x_6 = t. \tag{20}$$

Then, Eq. (19) will take the form of a power conic constraint as defined by the following expression:

$$x_4^{\alpha} x_5^{1-\alpha} \ge \sqrt{x_6^2}. \tag{21}$$

Accordingly, the optimization plane strain problem in the LB-FELA can be solved using the power conic programming (PCP) by imposing the GHB failure criterion as the summation of one quadratic conic constraint (Eq. 17) and one power conic constraint (Eq. 21).

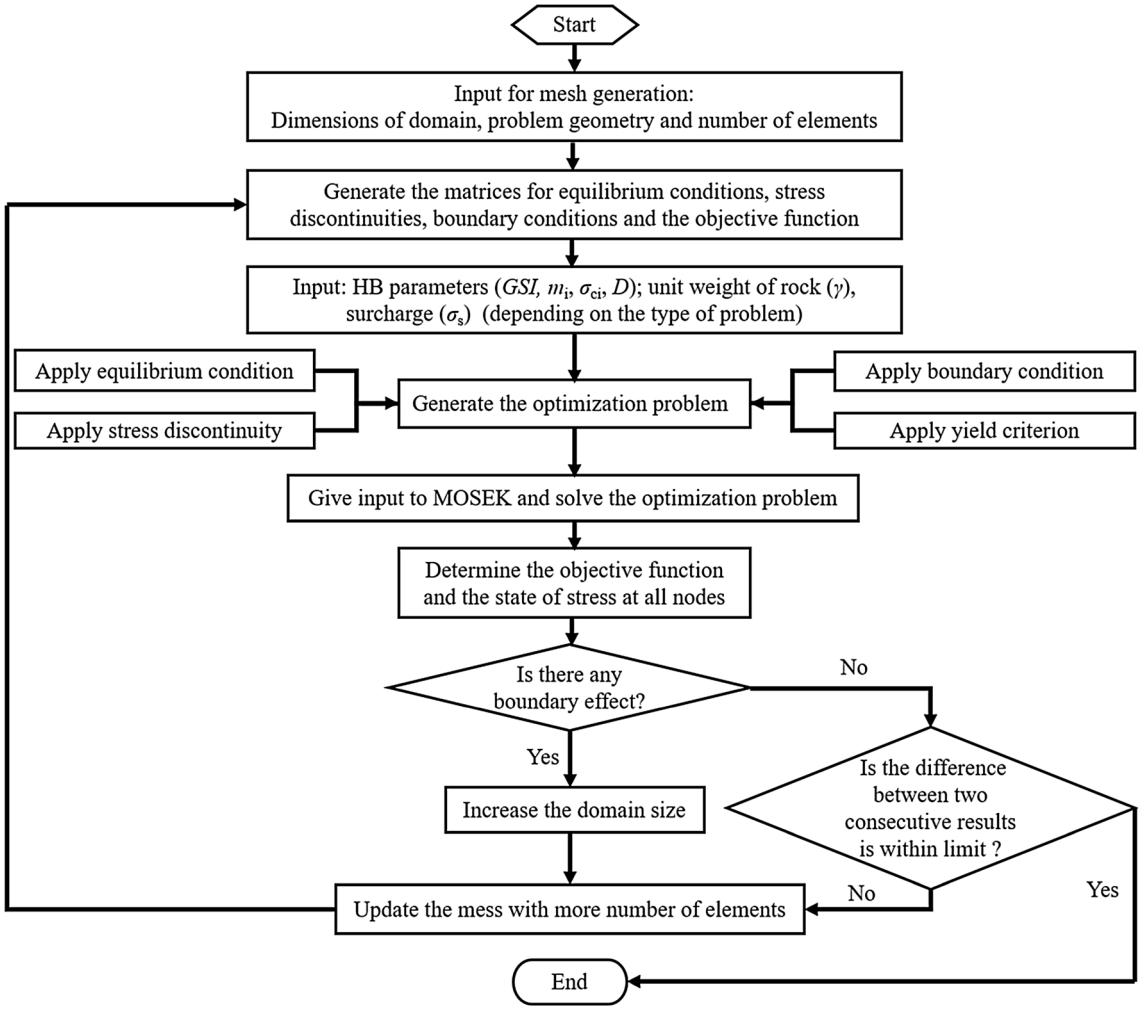

Fig. 2 A flow chart for performing the lower bound finite element limit analysis

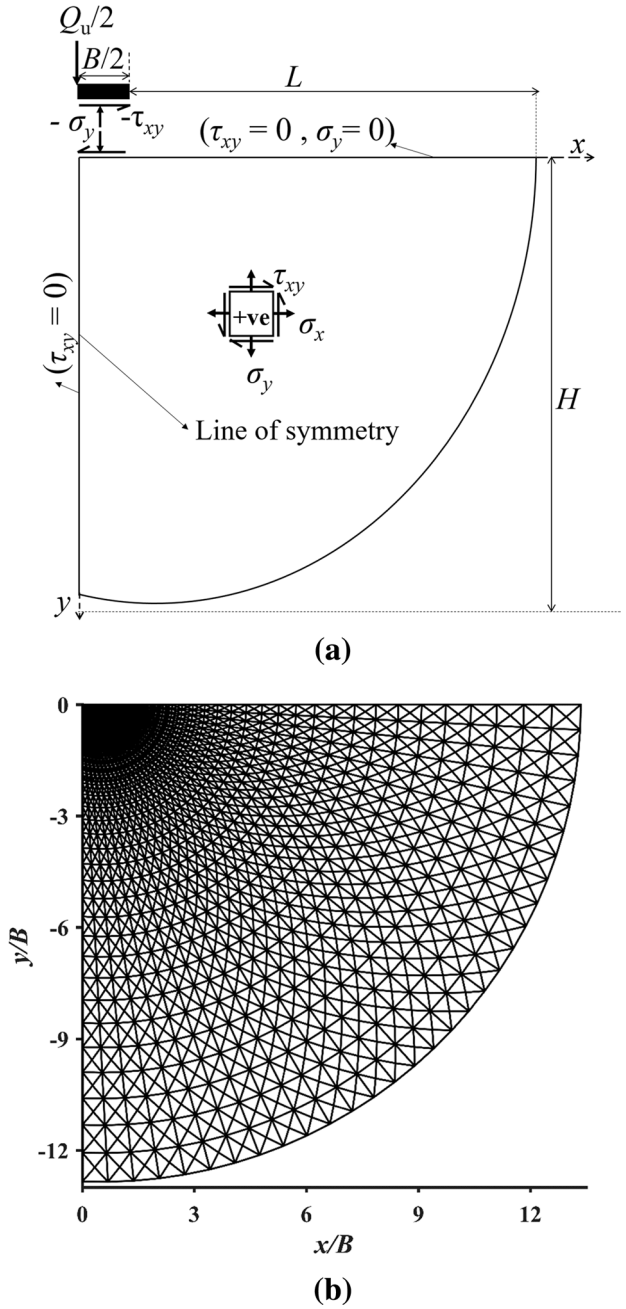

Fig. 3 For a strip footing: **a** stress boundary conditions, **b** a typical chosen mesh

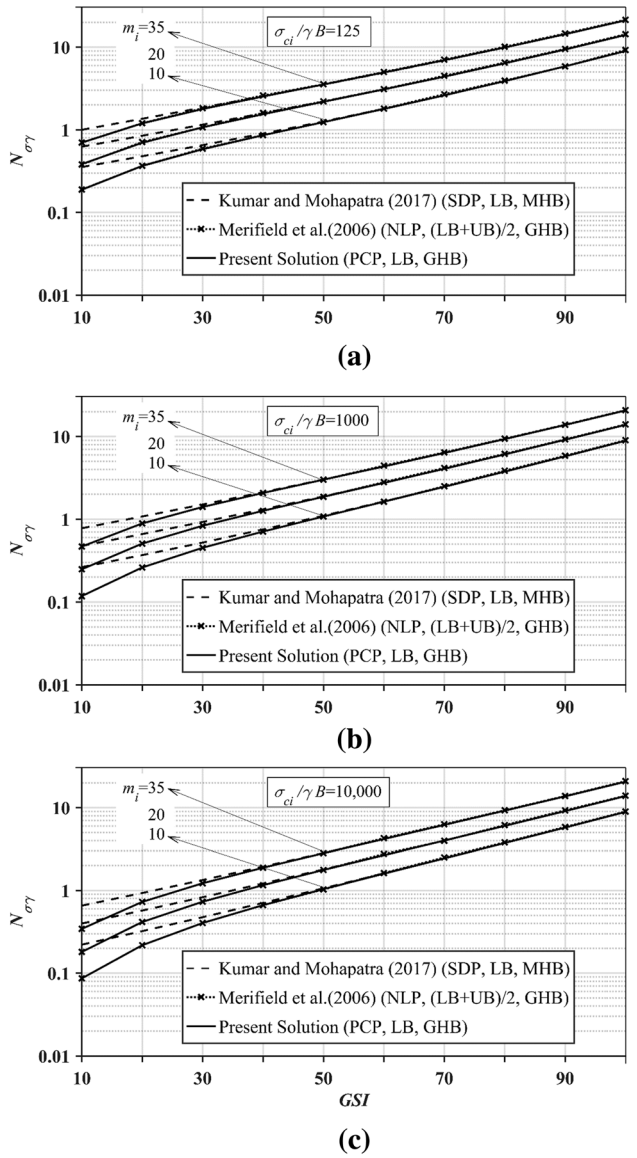

Fig. 4 For different values of GSI and m_i, a comparison of $N_{\sigma\gamma}$ using different methods for: **a** $\sigma_{ci}/\gamma B=125$; **b** $\sigma_{ci}/\gamma B=1000$; **c** $\sigma_{ci}/\gamma B=10{,}000$

6 Lower Bound (LB) Finite Elements Limit Analysis (FELA)

To discretize the selected domain, three-noded triangular elements have been used. Along the interfaces of all the elements, statically admissible stress discontinuities were being introduced. These stress discontinuities introduce additional degrees of freedom and help to attain a better lower bound solution. Following the lower bound limit analysis, the magnitude of the collapse load can be maximized by establishing a statically admissible stress field which should satisfy equilibrium conditions, the stress boundary conditions, the equations applicable along the stress discontinuities and nowhere it should violate the yield condition. The paper of Sloan (1988) can be referred for the derivation of the equations arising on account of the satisfaction of equilibrium conditions, stress discontinuities and boundary conditions. The enforcement of the GHB yield criterion has already been indicated by employing Eqs. (17) and (21).

Finally, the LB-FELA optimization formulation can be cast as a PCP problem in the following form:

$$\text{Maximize} \quad \mathbf{c}^{\mathrm{T}}\bar{\boldsymbol{\sigma}}. \tag{22}$$

Subjected to

$$\mathbf{A}_{\mathrm{equi}}\bar{\boldsymbol{\sigma}} = \mathbf{b}_{\mathrm{equi}}, \tag{23a}$$

$$\mathbf{A}_{\mathrm{dis}}\bar{\boldsymbol{\sigma}} = \mathbf{b}_{\mathrm{dis}}, \tag{23b}$$

$$\mathbf{A}_{\mathrm{bc}}\bar{\boldsymbol{\sigma}} = \mathbf{b}_{\mathrm{bc}}, \tag{23c}$$

$$\boldsymbol{f}(\bar{\boldsymbol{\sigma}}) \leq 0, \tag{24}$$

where $\mathbf{c}$ is a vector containing all the coefficient terms for the objective function, the vector $\bar{\boldsymbol{\sigma}}$ contains global unknown vector of the decision variables $[\bar{\sigma}]^{\mathrm{T}} = \left[\sigma^1\right]^{\mathrm{T}}\left[\sigma^2\right]^{\mathrm{T}} \cdots \left[\sigma^i\right]^{\mathrm{T}} \cdots \left[\sigma^{\mathrm{NN}}\right]^{\mathrm{T}}$, where NN denotes total number of nodes in the domain and $\sigma^i = [\sigma_x^i \sigma_y^i \tau_{xy}^i t^i x_1^i x_2^i x_3^i x_4^i x_5^i x_6^i]$. The constraints involving subscripts equi, dis and bc arise due to the satisfaction of equilibrium conditions, statically admissible stress discontinuities and stress boundary conditions, respectively. The inequality constraints associated with Eq. (24) arise due to the implementation of the GHB yield criterion. The working operation of the LB-FELA has also been explained by constructing a flow chart as illustrated in Fig. 2. The implementation of the PCP with the help of MOSEK has been explained in Appendix.

7 Numerical Examples for Stability Problems in Rock Mechanics

To demonstrate the efficacy of the present methodology, three different types of stability problems, as indicated earlier, were solved and the obtained results using the PCP were compared with that computed by employing the SDP and that reported on the basis of the NLP. The analysis was carried out on a desktop computer (Intel Core i7–7700 K CPU @ 4.20 GHz, 16 GB RAM) on the Windows 10 environment with the help of the conic programming toolbox MOSEK (version 9.0.84 2019) along with MATLAB version 2016. For all the problems chosen, the disturbance factor (D) in the GHB yield criterion was simply taken equal to 0.

7.1 Bearing Capacity of Strip Foundation on Rock Mass

A rigid strip footing of width B is placed on a semi-infinite rock media with horizontal free surface. The footing is rough and subjected to vertical downward load without any eccentricity. The interface of the footing and underlying rock mass

Table 1 A comparison of the bearing capacity factor (N_σ) for a rough strip footing with $\gamma = 0$

GSI	m_i	N_σ			GSI	m_i	N_σ		
		Merifield et al. (2006) NLP (LB + UB)/2	Kumar and Mohapatra (2017) SDP LB	Present analysis PCP LB			Merifield et al. (2006) NLP (LB + UB)/2	Kumar and Mohapatra (2017) SDP LB	Present analysis PCP LB
10	1	0.015	0.045	0.015	50	1	0.281	0.290	0.280
	5	0.042	0.123	0.042		5	0.644	0.662	0.643
	10	0.077	0.209	0.077		10	1.037	1.057	1.033
	20	0.156	0.369	0.154		20	1.765	1.781	1.754
	30	0.238	0.523	0.238		30	2.467	2.465	2.443
	35	0.288	0.599	0.284		35	2.817	2.796	2.786
20	1	0.044	0.071	0.044	70	1	0.765	0.776	0.763
	5	0.119	0.186	0.118		5	1.582	1.582	1.577
	10	0.209	0.312	0.208		10	2.444	2.438	2.438
	20	0.389	0.545	0.387		20	4.012	3.998	3.990
	30	0.575	0.768	0.571		30	5.491	5.460	5.452
	35	0.670	0.877	0.664		35	6.068	6.169	6.060
30	1	0.092	0.113	0.091	100	1	3.461	3.449	3.448
	5	0.235	0.283	0.234		5	6.124	6.104	6.103
	10	0.397	0.466	0.396		10	8.896	8.865	8.866
	20	0.713	0.806	0.707		20	13.847	13.790	13.790
	30	1.022	1.130	1.013		30	18.444	18.356	18.357
	35	1.193	1.289	1.186		35	20.688	20.553	20.553

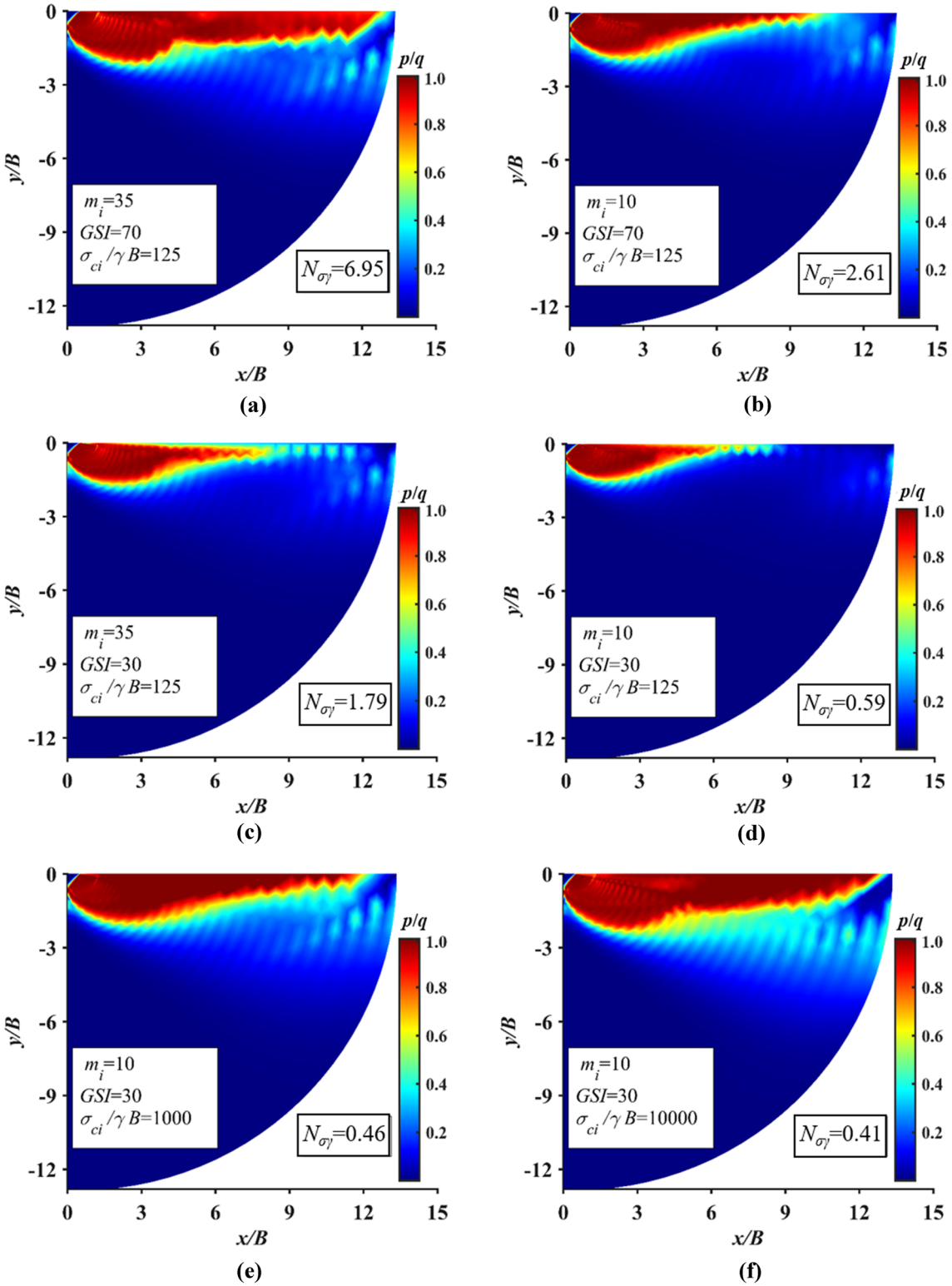

Fig. 5 Failure patterns for a strip footing for: **a** GSI = 70, $m_i = 35$ and $\sigma_{ci}/\gamma B = 125$; **b** GSI = 70, $m_i = 10$ and $\sigma_{ci}/\gamma B = 125$; **c** GSI = 30, $m_i = 35$ and $\sigma_{ci}/\gamma B = 125$; **d** GSI = 30, $m_i = 10$ and $\sigma_{ci}/\gamma B = 125$; **e** GSI = 30, $m_i = 10$ and $\sigma_{ci}/\gamma B = 1000$; **f** GSI = 30, $m_i = 10$ and $\sigma_{ci}/\gamma B = 10{,}000$

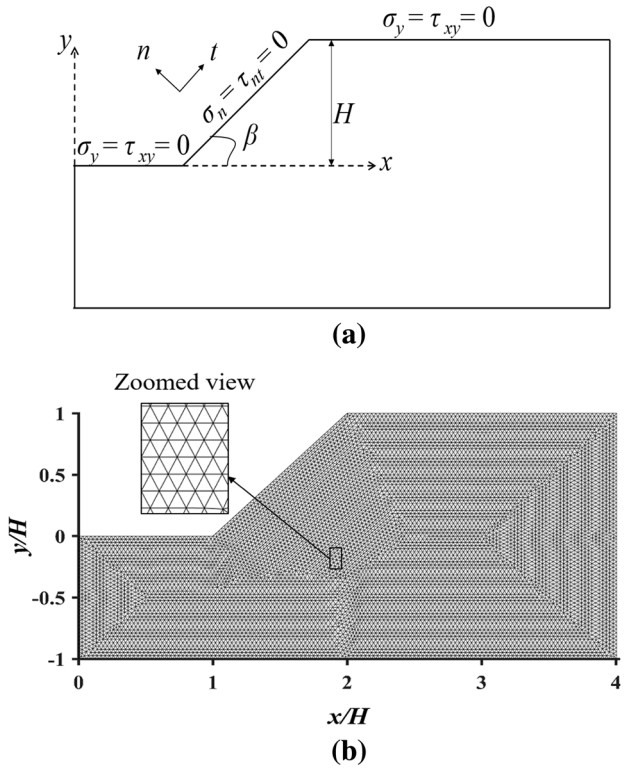

Fig. 6 For a finite slope: **a** stress boundary conditions; **b** a typical chosen mesh

is assumed to be the same as that of any plane within the rock media itself, as a result, no special provision needs to be made to simulate this footing–rock mass interface stress boundary condition. It is required to determine the maximum magnitude (Q_u) of the vertical load (objective function) which the rock media can withstand without failure. The bearing capacity factor ($N_{\sigma\gamma}$) is defined as:

$$N_{\sigma\gamma} = q_u/\sigma_{ci}, \tag{25}$$

where q_u is the ultimate bearing pressure which is equal to Q_u/B. The bearing capacity factor ($N_{\sigma\gamma}$) depends on (1) the different Hoek–Brown parameters GSI, m_i and σ_{ci}, (2) the unit weight of rock mass (γ) and the width of the foundation (B). The bearing capacity factor for a weightless ($\gamma = 0$) rock mass is simply denoted by N_σ. The chosen domain is shown in Fig. 3a; the size of the domain (L and H) are based on two primary requirements: (1) no yielding of the elements near the chosen boundaries of the domain and (2) a further extension of the chosen boundaries in either horizontal or vertical direction does not alter the results. The boundary conditions have been described in Fig. 3a. A typical mesh, with 6680 number of elements and 9950 discontinuities, has been illustrated in Fig. 3b. The fan-type mesh was chosen to account for the stress singularity along the footing edge.

The variation of $N_{\sigma\gamma}$ with an increase in GSI for three different values of m_i, namely 10, 20 and 35, corresponding to $\sigma_{ci}/(\gamma B) = 125$, 1000 and 10,000, is shown in Fig. 4a–c, respectively. It can be seen that the magnitude of $N_{\sigma\gamma}$ increases continuously with an increase in the values of both GSI and m_i. The magnitude of $N_{\sigma\gamma}$ becomes smaller for greater values of $\sigma_{ci}/(\gamma B)$. In all the cases, the results obtained from the present analysis were compared with (1) the average of lower and upper bound solutions given by Merifield et al. (2006) on the basis of the NLP for a given α, and (2) the lower bound solution of Kumar and Mohapatra (2017) using the SDP for $\alpha = 0.5$. It can be seen that for all the values of GSI and m_i, the present results with the application of the PCP match very closely with the solution given by Merifield et al. (2006), validating thereby the present solution procedure. Note that for the values of GSI < 40, the values of $N_{\sigma\gamma}$ reported by Kumar and Mohapatra (2017) for $\alpha = 0.5$ using the SDP become invariably greater than that on the basis of the present solution using the actual value of α and PCP. The difference between the two solutions increases continuously with a decrease in the value of GSI. It implies that for soft to very soft rocks, it will be unsafe to make an assumption of $\alpha = 0.5$.

To check the accuracy of the present solutions, the values of the bearing capacity factor N_σ for a weightless rock mass have been compared in Table 1 with the results of Merifield et al. (2006) on the basis of the NLP and Kumar and Mohapatra (2017) using an assumption of $\alpha = 0.5$. It can be noted that due to an assumption of $\alpha = 0.5$, Kumar and Mohapatra (2017) always overestimate the values of N_σ except for GSI = 100. The present solution also matches quiet well with the average of the LB and UB solution of Merifield et al. (2006).

The proximity of the state of stress to failure is defined on the basis of a ratio, p/q; where $p = (\sigma_1 - \sigma_3)$ and $q = (a'\sigma_1 + b')^\alpha$. The range of this ratio always lies between 0 and 1, and the value of $p/q = 1$ implies the yielding. The failure patterns' figures for a constant value of $\sigma_{ci}/(\gamma B) = 125$ with two different values of GSI, namely, 30 and 70 and for two different values of m_i, namely, 10 and 35, are shown in Fig. 5a–d. Also, with constant m_i and GSI, Fig. 5e, f display the failure patterns for $\sigma_{ci}/(\gamma B) = 1000$ and $\sigma_{ci}/(\gamma B) = 10000$, respectively. Note that in all the cases, starting from the center line, a curvilinear shape of the failure zone develops around the footing base and this zone extends right up to the ground surface. In all the cases, a small triangular non-plastic wedge develops below the footing base; this observation is similar to that usually noted for a rough strip footing with the usage of the MC yield criterion. Note that an increase in the values of GSI and $\sigma_{ci}/(\gamma B)$ leads to increase in the size of the plastic zone as well as the extent of the failure surface on the ground surface.

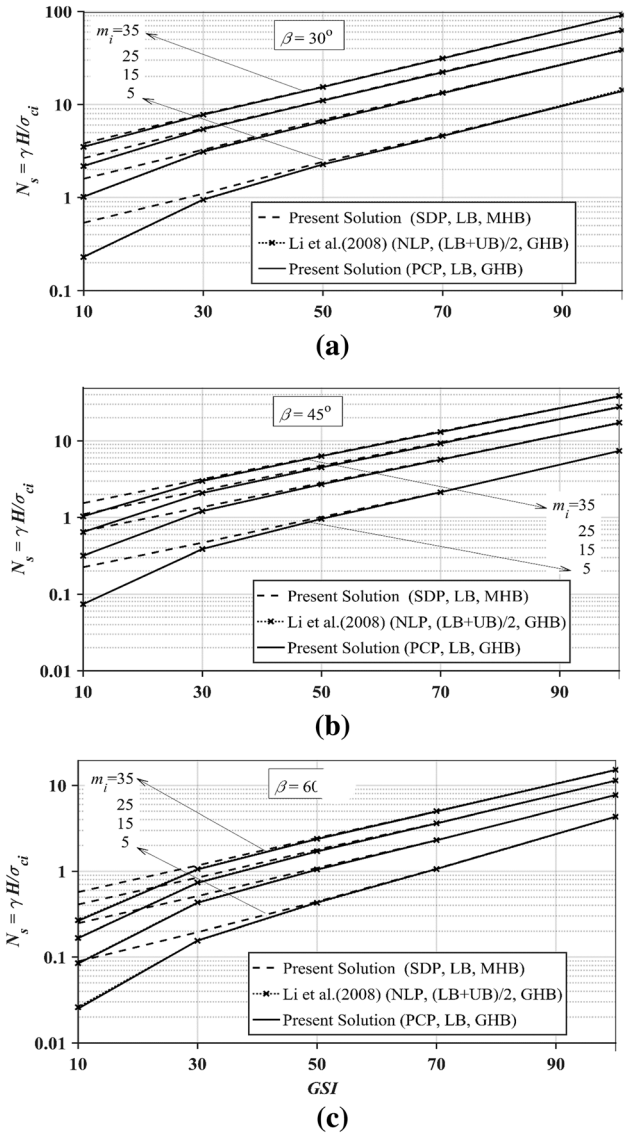

Fig. 7 A comparison of stability numbers for slopes with different GSI and m_i with: **a** $\beta = 30°$; **b** $\beta = 45°$; **c** $\beta = 60°$

7.2 Stability Analysis of Finite Rock Slopes

The geometry of the rock slope is shown in Fig. 6a. The slope is defined by means of two geometrical parameters: height (H) and slope angle (β). It is to maximise the magnitude of the unit weight (objective function) of a rock slope for (1) different values of H and β and (2) different input material properties of rock mass. Figure 6a gives the details of the boundary conditions which need to be imposed while solving this problem. A typical chosen mesh is presented in Fig. 6b. Depending on the geometry of the slope and properties of rock, the total number of elements was varied from 9500 to 28,200. All the numerical results were expressed in terms of a non-dimensional parameter, the stability number N_s which is defined as:

$$N_s = \gamma H/\sigma_{ci}. \tag{26}$$

The results were obtained for three different values of β, namely 30°, 45° and 60°. The variation of N_s for different combination of GSI and m_i has been shown in Fig. 7; four different values of m_i, namely, 5, 15, 25 and 35, were being chosen. Note that the magnitude of N_s increases continuously with an increase in the values of both GSI and m_i. Amongst the chosen values of β, the magnitude of N_s reduces with an increase in β; it is quite obvious since the stability of slopes will reduce with an increase in the slope angle (β). The obtained results are compared with the average of the LB and UB solutions published by Li et al. (2008) on the basis of the NLP. In addition, for the sake of comparison, the results were also obtained with the usage of the SDP for $\alpha = 0.5$. Note that the present results for the actual value of α on the basis of PCP matches very closely with the solution of Li et al. (2008). Like in the case of the foundation problem, the magnitude of N_s for $\alpha = 0.5$ with lower values of GSI becomes much greater than the corresponding result with the true value of α. Failure patterns for GSI = 90 and $m_i = 15$ with three different slope angles are shown in Fig. 8a–c. Irrespective of the slope angle, all these figures illustrate the toe failure. The size of the failure zone in terms of the normalized height increases continuously with a decrease in the slope angle.

7.3 Stability of Rectangular Unlined Tunnels in Rock Mass

A rectangular underground tunnel of height h, width w and cover H, as shown in Fig. 9a, has been considered for assessing its stability. Similar to the slope stability problem, it is to find the maximum unit weight (γ) of the rock mass for (1) different combinations of w, h and H, and (2) different values of GSI for a given m_i. The stress boundary conditions have been defined in Fig. 9a. Note that the interior perimeter of the tunnel is a surface free from any stress possibly due to either any lining or an anchorage device. A typical mesh has been shown in Fig. 9b. The stability number (N_t) for an underground tunnel is defined as:

$$N_t = \gamma H/\sigma_{ci}. \tag{27}$$

For $m_i = 15$, the variation of N_t with GSI for three different values of H/h, namely 1, 2 and 4 has been illustrated in Fig. 10a–c, respectively. Note that the value of N_t increases continuously with an increase in GSI. For a given GSI, the magnitude of N_t increases with an increase in the value of

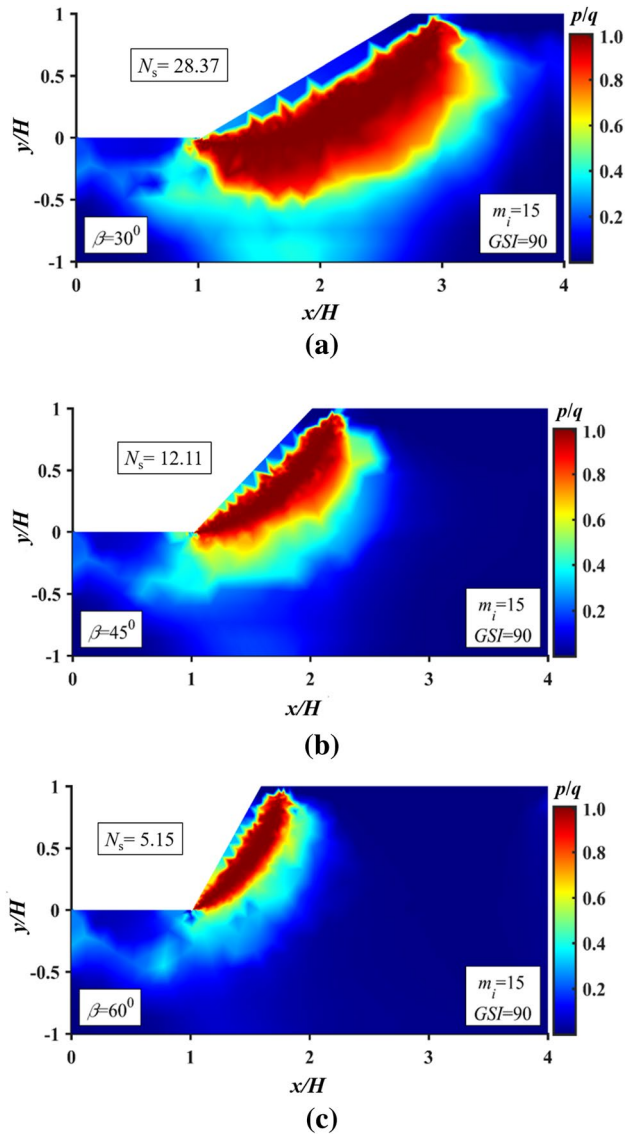

Fig. 8 For GSI=90 and m_i=15, the failure patterns for slopes with: **a** β=30°; **b** β=45°; **c** β=60°

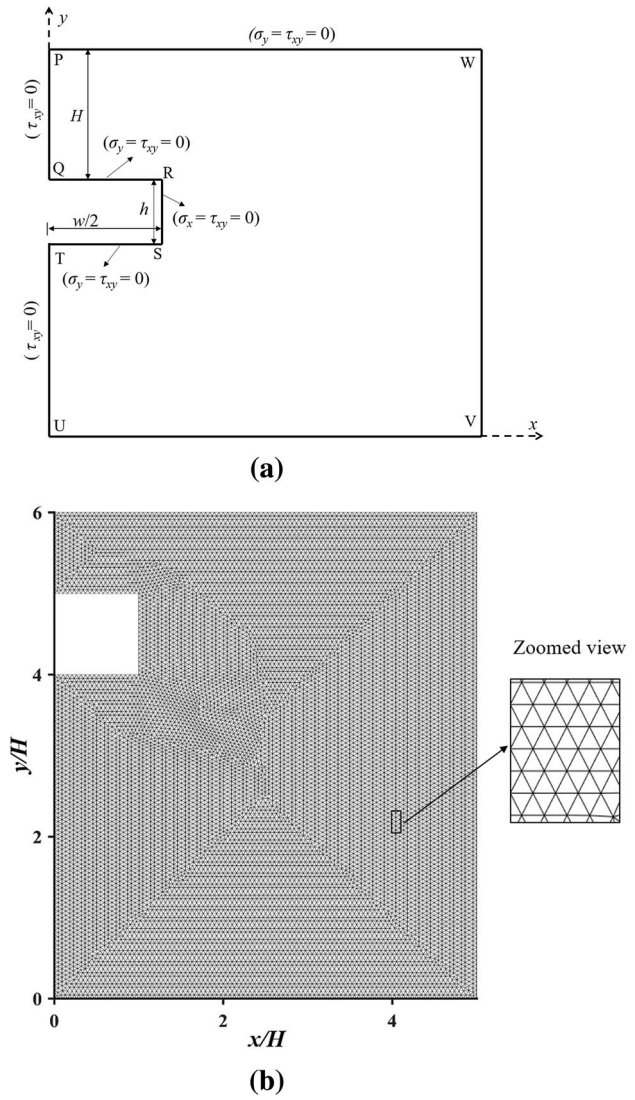

Fig. 9 For an unlined tunnel: **a** stress boundary conditions; **b** a typical chosen mesh

H/*h*. It implies that the stability of the tunnel for given values of *H* and *w*/*h* will improve with a decrease in the value of *h* which looks quite obvious. The magnitude of N_t increases with a decrease in the value of *w*/*h*; that is, for given values of *H* and *h*, the stability of the tunnel reduces with an increase in the width of the tunnel which also appears quite acceptable. The obtained solutions were compared for $\alpha = 0.5$, with the application of the SDP. Note that the value of N_t based on SDP is again found to be higher than the solution obtained from PCP. For the true value of α, depending on GSI, the obtained values of N_t were also compared with the average of lower and upper bound finite elements limit analysis solution on the basis NLP as reported by Suchowerska et al. (2012). Once again, it can be noted that in all the cases, the two solutions remain very close to each other.

Figure 11a–f illustrate the failure patterns for the tunnel problem. Figure 11a–c indicate the effect of *w*/*h*, using three different values, namely, *w*/*h* = 1, 2 and 4 with m_i = 15, GSI = 70 and *H*/*h* = 1. Starting from the upper edge of the tunnel, a curvilinear rupture zone develops which continuously progresses towards the vertical axis of the tunnel. Note that with an increase in *w*/*h*, the rupture zone gradually extends up to the ground surface. The effect of GSI on the failure patterns has been shown in Fig. 11d–f corresponding to m_i = 15, *w*/*h* =4 and *H*/*h* = 1. Note that with an increase in GSI not only the size of the rupture zone increases but also

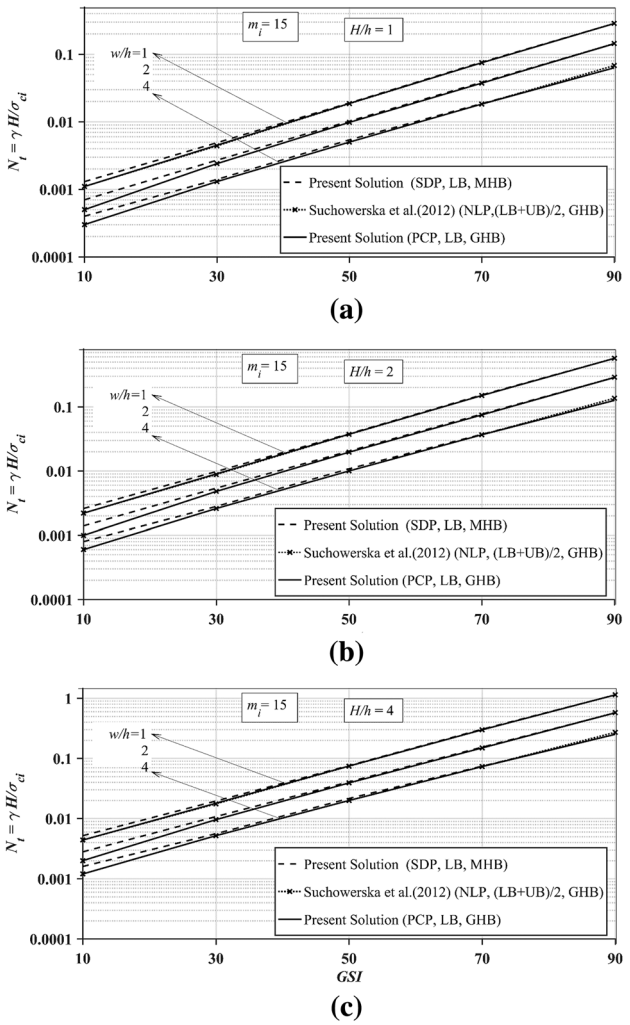

Fig. 10 For $m_i = 15$, a comparison of the stability numbers for tunnels with different values of GSI and *w/h* with: **a** $H/h = 1$; **b** $H/h = 2$; **c** $H/h = 4$

the rupture surface extends continuously up to the ground surface.

It should be mentioned that for the problems of foundations, slopes and tunnels taken in the Sects. 7.1, 7.2 and 7.3, the properties of the rock are defined by means of its material parameters GSI, m_i, D, γ and σ_{ci}. All the results have been normalized with respect to σ_{ci} and γ. It implies that one can simply generate the solution for any given magnitudes of σ_{ci} and γ. For the field application of the proposed method, one can either actually perform the analysis for given material parameters of the rock mass by incorporating the actual tunnel geometry or can even directly make of the proposed non-dimensional charts for the quick usage of the obtained results.

8 Mesh Dependency and Computational Efficiency of the Proposed Approach

As indicated earlier, the domain was discretized into a number of linear triangular elements. To examine the influence of the chosen mesh on the results, the solutions for all the three chosen problems were obtained for four different numbers of elements. The results with four different meshes for all three different types of problems are presented in Table 2; note that the total number of elements varies between 145 and 23,420. It can be noted that the values of $N_{\sigma\gamma}$, N_s and N_t increase continuously with an increase in the number of elements, and finally, the values of these non-dimensional factors, associated with the three different problems, tend to become constant. As was expected, the CPU times for running the programs increase continuously with an increase in the number of elements; observe that the CPU times vary between 0.65 and 43.94 s. To provide a comparison of the efficiency of present methodology on the basis of the PCP, for all the three chosen problems, the CPU times, along with the corresponding values of the bearing capacity factors/stability numbers, were also determined using the SDP formulations in combination with the iterative procedure of Kumar and Mohapatra (2018) corresponding to the true value of α. The results have been reported in Table 2 for different combinations of GSI and m_i. Note that the values of $N_{\sigma\gamma}$, N_s and N_t compare closely from both the methods. It can be noted that the current formulation using the PCP requires much lesser computational time than that with the usage of the SDP in conjunction with the iterative procedure to account for the true value of α. The difference between the CPU times associated with the present PCP approach and that on the basis of the SDP increases continuously with a decrease in the value of GSI; it should be mentioned that for lower values of GSI, greater number of steps is required to implement the iterative formulation of Kumar and Mohapatra (2018). The comparison clearly reveals the computational supremacy of the present PCP approach over the existing one without making any compromise with the accuracy. It should be mentioned that in the present analysis, three nodded triangular elements have been used. One can use higher-order elements with greater number of nodes. However, this will induce additional non-linearity in the analysis. No attempt has been made at present to obtain results using higher-order elements.

9 Conclusions

Using the generalized Hoek–Brown (GHB) yield criterion, a lower bound finite element limit analysis (LB-FELA) formulation has been introduced for solving different plane strain

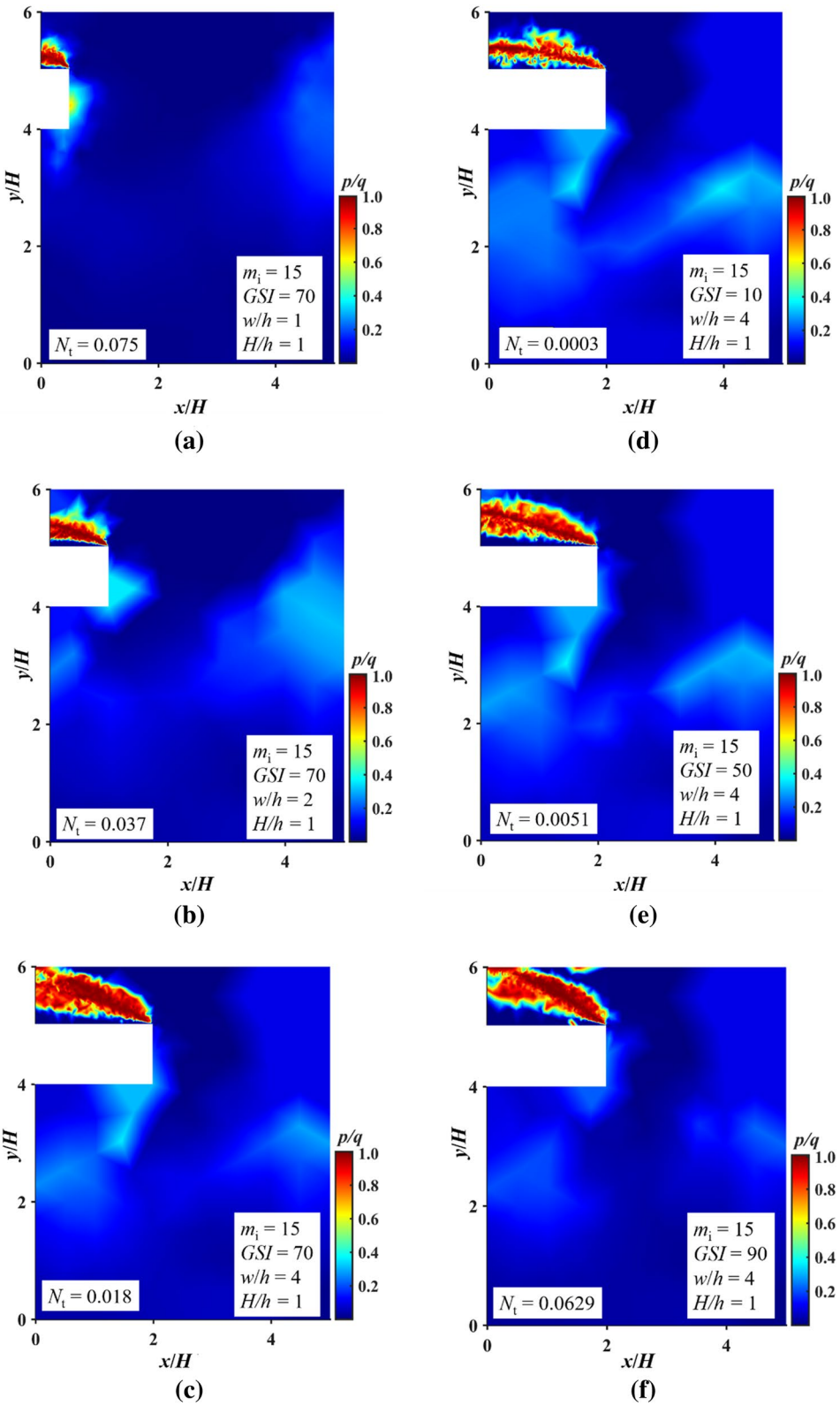

Fig. 11 Failure patterns for tunnels for $m_i = 15$, GSI = 70, $H/h = 1$ with: **a** $w/h = 1$; **b** $w/h = 2$; **c** $w/h = 4$ and $m_i = 15$, $H/h = 1$, $w/h = 4$; **d** GSI = 10; **e** GSI = 50; **f** GSI = 90

stability problems in rock mechanics on the basis of the power cone programming (PCP). The formulation considers the true value of the exponent in the GHB yield criterion. The proposed method does not require any assumption associated with either the value of the exponent in the GHB yield criterion or any smoothing of the yield surface. Accordingly,

the proposed technique overcomes the limitation and restriction of the optimization procedure in nonlinear programming and semi-definite programming technique which was followed till date. To show the efficacy of the proposed formulation, three different types of stability problems in rock mechanics have been analyzed: (1) determining the bearing capacity of strip foundation on rock mass, and (2) computing the stability numbers for finite rock slopes, and (3) evaluating the stability numbers of rectangular unlined tunnels in rock media. By applying the interior-point method based efficient algorithm using MOSEK, it is found that the application of the PCP in all the cases is computationally very versatile and it generates very accurate solution.

Appendix: Implementation of the PCP in MOSEK

The present investigation utilizes the optimization toolbox: MOSEK in MATLAB since it can handle the PCP which is found to be robust and computationally very efficient (Makrodimopoulos and Martin 2006; Ukritchon and Keawsawasvong 2018; Mohapatra and Kumar 2019a). To solve the PCP in MOSEK, the input needs to be specified in a particular way. The objective function, as given in Eq. (22), is defined by the command 'prob.c'. The matrices containing inequality or equality constraints are defined with 'prob.a' command. The lower and upper bounds of the constraints are specified by 'prob.blc' and 'prob.buc', respectively. The corresponding bounds on the variables are defined by 'prob.blx'

Table 2 A comparison of the results using the PCP and the SDP formulations for different chosen problems

Problem	GSI	m_i	Other parameters	NE	Optimization method			
					Present method		Kumar and Mohapatra (2018)	
					PCP GHB		SDP + iterative method GHB	
					$N_{\sigma\gamma}$	CPU (s)	$N_{\sigma\gamma}$	CPU (s)
Strip footing	10	5	$\sigma_{ci}/(\gamma B)=125$	145	0.076	0.65	0.088	12.60
				1515	0.090	5.14	0.103	108.34
				5250	0.095	16.17	0.108	361.20
				8550	0.096	21.31	0.110	497.42
	30	20		1435	1.025	4.53	1.032	76.84
				5550	1.061	16.86	1.069	344.52
				11,290	1.067	29.78	1.074	526.71
				14,790	1.070	34.85	1.078	801.24
					N_s	CPU (s)	N_s	CPU (s)
Finite slope	10	5	$\beta=60°$	584	0.014	1.92	0.016	40.41
				3304	0.020	9.61	0.023	194.52
				10,524	0.023	25.25	0.027	570.78
				15,146	0.025	31.15	0.029	767.20
	70	35		954	2.583	2.88	2.824	46.28
				5772	3.945	15.50	4.124	255.80
				15,801	4.645	34.66	4.656	560.80
				23,420	5.104	43.94	5.108	667.45
					N_t	CPU (s)	N_t	CPU (s)
Rectangular tunnel	10	15	$H/h=1$, $w/h=1$	348	0.0004	1.12	0.0006	28.32
				3542	0.0006	10.10	0.0008	244.13
				5634	0.0008	15.24	0.0009	398.47
				9753	0.0009	23.68	0.0010	711.10
	90	15		1346	0.1066	2.96	0.1070	7.12
				8680	0.1475	21.24	0.1477	50.40
				13,942	0.1651	29.68	0.1653	87.34
				19,864	0.1892	40.24	0.1892	102.24

and 'prob.bux'. The cones are prescribed using four different cell arrays: 'prob.cones.type', 'prob.cones.conepar', 'prob.cones.sub' and 'prob.cones.subptr'. The array 'prob.cones.type' specifies the type of cone and it takes the command (1) 'res.symbcon.MSK_CT_QUAD' for the second-order cone, (2) 'res.symbcon.MSK_CT_RQUAD' for the rotated quadratic cone, and (3) 'res.symbcon.MSK_CT_PPOW' for the power cone. The value of the power term in the power cone is specified by 'prob.cones.conepar'. The variables related to a particular cone are specified by 'prob.cones.sub' and the change in the cone is indicated in 'prob.cones.subptr'. The optimal solution of the objective function is obtained through 'res.sol.itr.pobjval' command. The primal as well as dual optimal solutions of the variables are finally reported in 'res.sol.itr.xx' and 'res.sol.itr.y', respectively.

References

Alizadeh F (1995) Interior point methods in semidefinite programming with applications to combinational optimization. SIAM J Optim 5(1):13–51

Alizadeh F, Goldfarb D (2003) Second-order cone programming. Math Progr Ser B 95(1):3–51

Alzoubi AK, Martin CD, Cruden DM (2010) Influence of tensile strength on toppling failure in centrifuge tests. Int J Rock Mech Min Sci 47:974–982

Andersen ED, Roos C, Terlaky T (2003) On implementing a primal-dual interior-point method for conic quadratic optimization. Math Progr 95(2):249–277

Boyd S, Vandenberghe L (2004) Convex optimization. Cambridge University Press, Cambridge

Chakraborty M, Kumar J (2015) Bearing capacity of circular footings over rock mass by using axisymmetric quasi lower bound finite element limit analysis. Comput Geotech 70:138–149

Cundall PA (1971) A computer model for simulating progressive large scale movements in blocky rock systems. In: Proceedings of the international symposium on rock fracture, Nancy, October 1971. International society for rock mechanics (ISRM), 1, paper no. II–8, pp 129–136

Hoek E (1983) Strength of jointed rock masses. Geotechnique 33(3):187–223

Hoek E (2007) Practical rock engineering. http://www.rocscience.com

Hoek E, Brown ET (1980) Empirical strength criterion for rock masses. J Geotech Eng Div 106(GT9):1013–1035

Hoek E, Carranza-Torres C, Corkum B (2002) Hoek–Brown failure criterion 2002 edition. In: Proceedings of the 5th North American Rock mechanics symposium and the 17th Tunnelling Association of Canada Conference: NARMS-TAC, Toronto

Krabbenhoft K, Lyamin AV, Sloan SW (2007) Formulation and solution of some plasticity problems as conic programs. Int J Solids Struct 44(5):1533–1549

Kumar J, Mohapatra D (2017) Lower-bound finite elements limit analysis for Hoek–Brown materials using semidefinite programming. J Eng Mech 143(9):04017077

Kumar J, Mohapatra D (2018) Closure to lower bound finite elements limit analysis for Hoek–Brown materials using semidefinite programming by J Kumar and D Mohapatra. J Eng Mech 144(7):07018002

Li AJ, Merifield RS, Lyamin AV (2008) Stability charts for rock slopes based on the Hoek–Brown failure criterion. Int J Rock Mech Min Sci 45(5):689–700

Li LC, Tang CA, Zhu WC, Liang ZZ (2009) Numerical analysis of slope stability based on the gravity increase method. Comput Geotech 36:1246–1258

Lian JJ, Li Q, Deng XF, Zhao GF, Chen ZY (2018) A numerical study on toppling failure of a jointed rock slope by using the distinct lattice spring model. Rock Mech Rock Eng 51(2):513–530

Makrodimopoulos A, Martin CM (2006) Lower bound limit analysis of cohesive frictional materials using second-order cone programming. Int J Numer Methods Eng 66(4):604–634

Merifield RS, Lyamin AV, Sloan SW (2006) Limit analysis solutions for the bearing capacity of rock masses using the generalized Hoek–Brown yield criterion. Int J Rock Mech Min Sci 43(6):920–937

Mohapatra D, Kumar J (2019a) Smoothed finite element approach for kinematic limit analysis of cohesive frictional materials. Eur J Mech A Solids 76:328–345

Mohapatra D, Kumar J (2019b) Collapse loads for rectangular foundations by three dimensional upper bound limit analysis using radial point interpolation method. Int J Numer Anal Methods Geomech 43(2):641–660

MOSEK ApS (2019) The MOSEK optimization tools manual version. http://www.mosek.com

Nesterov YE, Todd MJ (1998) Primal-dual interior-point methods for self-scaled cones. SIAM J Optim 8(2):324–364

Shi GH, Goodman RE (1985) Two dimensional discontinuous deformation analysis. Int J Numer Anal Meth Geomech 9(6):541–556

Sloan SW (1988) Lower bound limit analysis using finite elements and linear programming. Int J Numer Anal Methods Geomech 12:61–77

Sloan SW (2013) Geotechnical stability analysis. Géotechique 63(7):531

Sturm JF (1999) Using SeDuMi 1.02, a MATLAB toolbox for optimization over symmetric cones. Optim Methods Soft 11(1–4):625–653

Suchowerska AM, Merifield RS, Carter JP, Clausen J (2012) Prediction of underground cavity roof collapse using the Hoek–Brown failure criterion. Comput Geotech 44:93–103

Swan CC, Seo Y (1999) Limit state analysis of earthen slopes using dual continuum/FEM approaches. Int J Numer Anal Methods Geomech 23(12):1359–1371

Tang C, Toh K, Phoon K (2014) Axisymmetric lower-bound limit analysis using finite elements and second order cone programming (SOCP). J Eng Mech 140(2):268–278

Tütüncü RH, Toh KC, Todd MJ (2003) Solving semidefinite-quadratic-linear programs using SDPT3. Math Progr 95(2):189–217

Ukritchon B, Keawsawasvong S (2018) Three-dimensional lower bound finite element limit analysis of Hoek–Brown material using semidefinite programming. Comput Geotech 104:248–270

Ukritchon B, Keawsawasvong S (2019) Stability of unlined square tunnels in Hoek–Brown rock masses based on lower bound analysis. Comput Geotech 105:249–264

Zhang R, Chen G, Zou J, Zhao L, Jiang C (2019) Study on roof collapse of deep circular cavities in jointed rock masses using adaptive finite element limit analysis. Comput Geotech 111:42–55

Zienkiewicz OC, Humpheson C, Lewis RW (1975) Associated and nonassociated viscoplasticity in soil mechanics. Géotechnique 25(4):671–689